Dynamics of Slow Drainage in Porous Media

Knut Jørgen Måløy, Liv Furuberg, Jens Feder, and Torstein Jøssang
Department of Physics, University of Oslo, Box 1048, Blindern, 0316 Oslo 3, Norway
(Received 11 July 1991)

Pressure fluctuations measured during slow drainage in a two-dimensional porous model exhibit sudden jumps that identify bursts where the invasion front proceeds abruptly. The pressure jump size distribution is observed to be exponential. The nonscaling dynamics created fractal fronts and invaded regions described by invasion percolation. A new modified invasion percolation algorithm includes invasion dynamics. A capacitive volume associated with each interface throat results in a crossover from power-law behavior to an exponential pressure jump distribution consistent with observations.

PACS numbers: 47.55.Mh, 05.40.+j, 47.55.Kf

Immiscible fluid-fluid displacement in porous media generates front structures and patterns [1,2] ranging from the compact to the ramified and fractal [3]. Fractal structures are generated when a nonwetting fluid is injected into a wetting fluid (drainage) at low injection rates [1]. Recently both simulations and experiments [4–6] were performed to examine the *dynamics* in the high velocity, viscous fingering regime. At low injection rates, where capillary forces dominate, few [6] experiments studied the front *dynamics*. Simulations [7,8] based on the invasion percolation algorithm [9] did not have a physically realistic time variable.

Early qualitative observations [10–12] of slow displacement dynamics showed that displacement occurred in a discontinuous way. On the pore level the interface between the fluids deformed continuously for a while, but occasionally the interface became unstable and many pores were displaced in a burst [see Figs. 1(a)–1(c)]. These bursts were accompanied by sudden jumps in the pressure difference (capillary pressure) between the invading and the defending fluids, so-called "Haines jumps" [10] (see Fig. 1). Thompson, Katz, and Raschke [13] measured jumps in electrical resistance in mercury intrusion experiments in three-dimensional porous media. They found a power-law distribution of the resistance jumps consistent with simulations [14,15]. However, not all Haines jumps are observed, because injection into dead ends of the mercury cluster are not observed in the resistance.

In recent simulations of the *dynamics* of invasion percolation [7,8] a burst was defined geometrically as the number of pores invaded from one pore on the interface before invasion stops and continues elsewhere. The burst size distribution was found to have a scaling behavior. Roux and Guyon [8] introduced a new (hierarchical) definition of bursts and found a power-law distribution of the burst sizes, with exponents related to percolation exponents [16]. Gouyet [17] simulated drainage in a gravitational field, and by considering fluctuations of the front he obtained a similar burst distribution.

We present for the first time *measurements* and *simulations* of pressure fluctuations during drainage of water by air in two-dimensional porous models. We also measured the intervals between pressure jumps corresponding to bursts. The distributions of both pressure jump sizes and intervals were not scaling but approximately exponential (see Fig. 2). We introduce a modified invasion percolation algorithm that includes a *capacitive interface volume* and models the constant rate experiment with a physical time and pressure. Using parameters estimated from experiments, we obtain distributions for pressure jumps and intervals in good agreement with observations (see Fig. 2). Moreover, we conclude from the simulations that the observed exponential distributions are crossover effects from power-law distributions (Fig. 3) expected, for example, when the surface tension is decreased, the pore sizes increased, or for larger systems.

In our experiments we used a 120×175-mm transparent porous model [4,5] that consisted of a random monolayer of 1-mm glass beads sandwiched between plastic sheets. The model had a porosity $\phi \simeq 0.7$ and average pore volume $\Omega = 2\ \mathrm{mm}^3$. Water was withdrawn from one short side of the model with a syringe pump at a low *constant rate* of $Q = 0.048$ pore/s. Pressure fluctuations were measured with a pressure sensor of our own construction, having a resolution of 0.1 mm H_2O. An experiment consisted of about 70000 pressure measurements taken at 1-s intervals; see Fig. 1.

We observed that in periods when the water interface was in capillary equilibrium, the extraction of water at a constant rate did not immediately lead to air displacing water from pores. Instead the interface was sucked into narrower parts of the throats between the pores because of the larger capillary pressure and invading air accumulated on the air side of the menisci in the throats. The capillary pressure is related to the radius of the front at the position of the meniscus by $p_{\mathrm{cap}} = \sigma(R_1^{-1} + R_2^{-1})$, where σ is the interface tension and R_1 and R_2 are the principal radii of curvature. The capillary pressure increased with time between jumps at an average rate $\Gamma = dp_{\mathrm{cap}}/dt = Q/n_f K$, where n_f was the length of the front in terms of the number of pore throats in the front [$n_f = 4$ and 9 in Figs. 1(a) and 1(b), respectively], and $K^{-1} = dp_{\mathrm{cap}}/dv$, with $dv = (Q/n_f)dt$ the water displaced

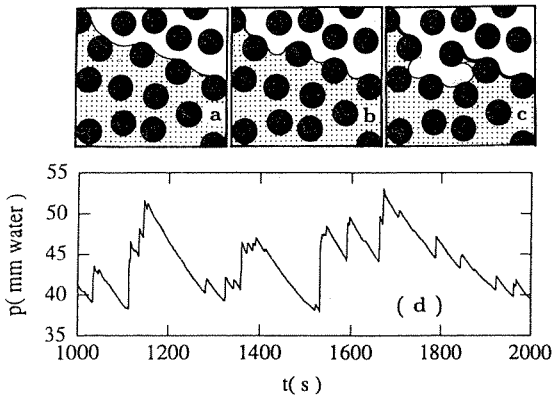

FIG. 1. (a)–(c) Invasion of air (white) into a two-dimensional porous medium filled with water. As water is extracted, the interface moves into narrower parts of the throats. During a burst new pores are invaded and the interface adjusts everywhere to the lower capillary pressure. The heavy black lines show the redistributed volume. (d) Pressure in the water during drainage as a function of time.

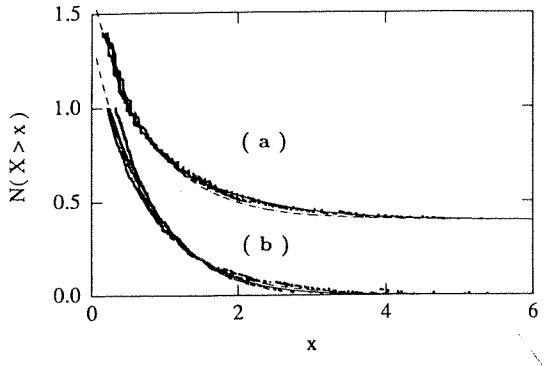

FIG. 2. (a) Cumulative distribution of intervals between subsequent bursts, $X=T$. Distributions in (a) are vertically shifted by 0.4. (b) Cumulative distribution of pressure jumps, $X=P$. Data from three different experiments are shown as points, simulations as a solid line, and the exponential function as a dot-dashed line. The best experimental fits by the function $C\exp(-\beta X)$ are $\beta=1.27$ in (a) and $\beta=1.31$ in (b).

in a typical pore throat in time dt. For the results shown in Fig. 1(d), $K\simeq 5.5\times 10^{-3}$ pore/mm H_2O and $n_f\simeq 100$. The slight curvature in quasiequilibrium increases of the capillary pressure is ignored in the following discussion. When the capillary pressure exceeded the smallest capillary pressure threshold of throats connecting invaded and noninvaded pores, the front became unstable and invaded through the weak (widest) throat. The displaced water volume was distributed back over the front, the invading air retreated everywhere slightly, and the capillary pressure correspondingly decreased. At this stage the invasion process continued if any of the freshly exposed pore throats were unstable. Thus an instability at a given pore throat could trigger an avalanche of pore invasions with an accompanying abrupt decrease in the capillary pressure [see Fig. 1(d)]. The avalanche ended when capillary equilibrium had been reestablished. The pressure drop had a time scale set by viscosity and was effectively instantaneous for our experiment. The dynamics of the process depended on the typical pore volume Ω, the number s of pores invaded, and details of the pore geometry that determines how the displaced volume is distributed over the front.

In Fig. 2(a) we show the cumulative distribution of jumps in capillary pressure and in Fig. 2(b) the cumulative distribution of the interval between pressure jumps. The observed distributions are almost exponential and well described by the simulations described below.

A square lattice of size $L_1\times L_2$ that consisted of nodes (pores) connected by bonds (throats) represented the porous medium in the simulations. The invasion process started with all pores occupied by the defending fluid (water) and with the leftmost column of pores invaded by air. Bonds were assigned random numbers p_i drawn from a uniform distribution on [0,1] representing capillary pressure thresholds in the throats. As in ordinary invasion percolation (IP) [9] one searched for the bond with the lowest value of p_i ($p_{i,\min}$) among the bonds that connect invaded pores to pores that are not invaded or trapped. But contrary to ordinary IP a bond and the connected site were not invaded at each time step. Instead one increased the time variable before any invasion took place by the time needed to increase the capillary pressure from the present value (initially $p_{\rm cap}=0$) to $p_{i,\min}$: $t=t_0+(p_{i,\min}-p_{\rm cap})n_fK$. The number of throats at the interface n_f was initially equal to the width of the system L_1. After a transition period the value of n_f fluctuated around a value [18] scaling with L_1 as $n_f\sim L_1^{D_e}$, with $D_e\simeq 1.39$.

A burst was defined to start as the widest available bond with $p_i=p_{i,\min}$ and the connected pore were invaded after the capillary pressure had built up. In the new algorithm all pores had been assigned a random number V_i, uniformly distributed in $[\frac{1}{2},\frac{3}{2}]$ representing pore volumes. This simple distribution gives an average volume of 1, and is sufficient for modeling the nonextreme experimental distribution which has an average pore volume. The experimental volumes are always greater than zero. The invasion of a pore with a volume V_i resulted in a decrease in the capillary pressure to $p_{\rm cap}=p_{i,\min}-V_i/n_fK$. Again the available bond with the lowest value of the capillary pressure threshold was found on the new front. If this $p_{i,\min}$ was larger than $p_{\rm cap}$, the capillary pressure had to be increased again, leading to a new increase of the time variable and the beginning of a new burst. If, on the contrary, $p_{i,\min}$ was smaller than $p_{\rm cap}$, this bond and the connected site could be immediately invaded in the present burst, leading to a further decrease of the capillary pressure but no increase of the time. The burst continued until the capillary pressure was too small to invade any of the available throats. Thus the total capillary

pressure change in a burst is

$$\Pi = -\sum_i V_i/n_f K , \quad (1)$$

where the sum is over all pores invaded in the burst.

Figure 3 shows results obtained from simulations on $L_1 = 200$, $L_2 = 1500$ lattices for different values of K. The data were collected only after the front length stabilized. The pressure jump size distribution $n(\Pi)$ was assumed to have a scaling form

$$n(\Pi) = \Pi^{-\hat{\tau}} f(\Pi/\Pi^*)(n_f K)^{(1-\hat{\tau})}, \quad (2)$$

where $\Pi^* \sim (n_f K)^{-a}$. The crossover function $f(x)$, which is a constant for $x \ll 1$ and vanishes quickly as $x \to \infty$, is plotted in Fig. 3. The best fit was obtained for $\hat{\tau} = 1.30 \pm 0.05$ and $a = 0.3 \pm 0.05$.

The exponents $\hat{\tau}$ and a can be expressed by static exponents of percolation and invasion percolation. The arguments for these relations use the one-to-one correspondence between our capillary pressure $p_{\rm cap}$ and the fraction of occupied sites in normal percolation. This correspondence is caused by our uniformly distributed capillary pressure thresholds. The geometric size of the bursts in terms of the number of invaded sites is roughly related to the pressure jumps by $s \simeq \Pi n_f K$. This gives a scaling form for the distribution of geometric burst sizes: $n(s) = s^{-\hat{\tau}} f(s/s^*)$, where s^* is the characteristic burst size. In the following we assume that the size of the lattice is much larger than the characteristic length introduced by the capacitive volume effect.

A parallel argument to that of Roux and Guyon for the size distribution exponent [8] $\hat{\tau}$ of invasion percolation with trapping applies also in our case. We define the *burst capillary thresholds* in our simulations as the subset of capillary threshold pressures at which a burst starts. The burst capillary thresholds are distributed narrowly around p_c when $Kn_f \to \infty$, which is the limit where the pressure does not decrease during a burst and the burst size distribution is a power law as in normal invasion percolation. Using that all bursts start at p_c in this limiting case and that our simulations have a different trapping rule than that of Roux and Guyon, we obtain [8] $\hat{\tau} = -D_e/D + D/D'(\tau - 1) + 1 = 1.35$, where D_e is the fractal dimension of the external perimeter, $D' = 1.89$ is the fractal dimension of invasion percolation without trapping, and $\tau = 2.07$ is the cluster size distribution exponent for percolation. The characteristic burst size s^* and the corresponding characteristic linear burst size $s^{*1/D}$ depend on the strength of the capacitive volume-pressure effect and the length of the absorbing front. Considering bursts starting at the critical pressure p_c [16], the pressure decreases from p_c as pores are invaded, and we expect the crossover length to be visible when the correlation length ξ is equal to the characteristic extent of bursts. This corresponds to the pressure drop Π:

$$\Pi^{-\nu} \sim (p_c - p_{\rm cap})^{-\nu} \sim (s/n_f K)^{-\nu} \sim \xi \sim s^{1/D}$$

($\nu = 1.34$ is the correlation exponent for percolation [16] and $D = 1.82$ is the measured fractal dimension [9] of the invasion percolation cluster). The scaling of a typical cluster size and pressure jump thus becomes

$$s^* = (Kn_f)^{\nu D/(1+\nu D)}, \quad \Pi^* = (Kn_f)^{-1/(1+\nu D)}, \quad (3)$$

where the numerical value of $a = 1/(1+\nu D)$ is 0.29 as observed.

Figure 2 shows the exponential and corresponding numerical burst capillary pressure distributions. We have

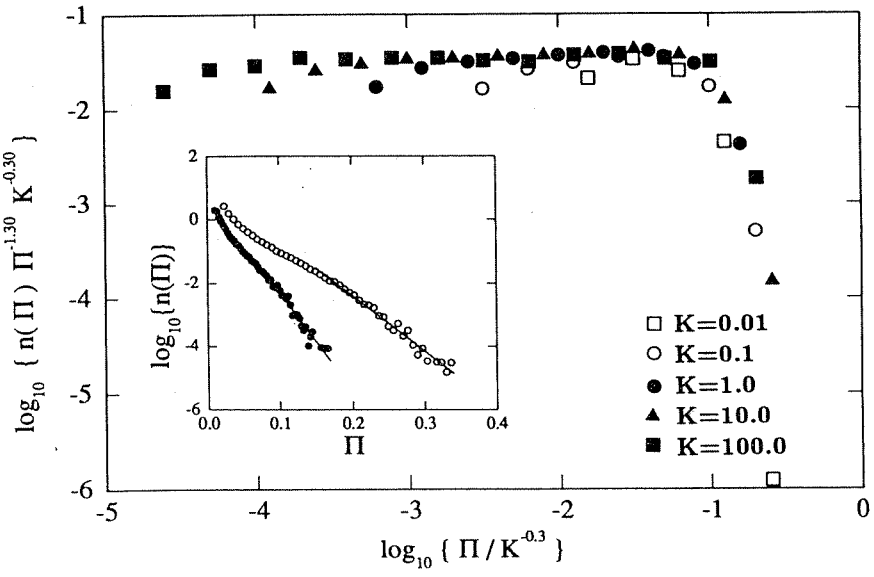

FIG. 3. Crossover function for the pressure jump distribution. The five curves correspond to $K = 0.01$, 0.1, 1, 10, and 100. For each value of K the points represent averages over five independent simulations on 200×1500 lattices. Inset: The exponential regime, in detail, for $K = 0.1$ and $K = 1$.

estimated the experimental value of K from the slope of the experimental pressure to time curve. The water-air front is initially flat, giving $n_f \simeq 100$ for the first buildup regions. The extraction rate gives $0.048\delta t$ pores invaded during an interval δt. The pressure differences measured in the experiment cannot be directly compared to pressure differences in the simulations, since the capillary pressure threshold distribution of the porous medium is unknown. We measure burst capillary threshold values in simulations in the range 0–0.55, while the corresponding experimental pressures are approximately in the range of 0–16 mm H_2O. If we assume a uniform capillary threshold distribution in the porous medium, we estimate the following relation between the experimentally measured pressures p and the corresponding simulation pressures p_{cap}: $p_{cap} = 0.034p/(\text{mm } H_2O)$. By comparing the burst capillary threshold distributions for simulations and experiments we find a good consistency and conclude that the capillary threshold distribution in the porous medium is well described by a uniform distribution in the range of pressures that dominates the process. Using the linear relation between simulated and experimental pressures, we obtain $K \simeq 0.2$.

We performed 100 simulations where we used this value of K, a lattice of $L_1 = 100$ and $L_2 = 200$ corresponding to the experimental model, and stopped the simulations after 750 bursts, which is the typical total number of bursts in an experiment. Figure 2 shows the exponentially decreasing cumulative pressure jump distributions for three different experiments together with simulations and an exponentially decreasing curve. Pressures $P = \Pi/\langle\Pi\rangle$ are divided by $\langle\Pi\rangle$ which is the mean value of the pressure jumps Π above the experimental resolution of 0.1 mm H_2O.

Also the cumulative distributions of Δt, the intervals between subsequent bursts, are shown in Fig. 2 for both experiments and simulations, using the dimensionless times $T = \Delta t/\langle\Delta t\rangle$. $\langle\Delta t\rangle$ is the mean value of the buildup time, averaged over all times larger than the time it takes to build up the pressure corresponding to a capacitive volume of one typical pore volume. For times shorter than this the buildup time distribution is not expected to be correct because it will strongly depend on the distribution of the detailed pore volume.

In conclusion, we find close agreement between simulations and experiments. Since both the pressure jump distribution and the buildup time distribution show exponential decay, we conclude that the capillary pressure in the experiments depends strongly on the capacitive interface volume and that the experiments are in the crossover regime. We find a fractal structure that arises by a dynamic process that is not characterized by power laws, but by exponential functions. In the limit when $Kn_f \to \infty$ the dynamics is governed by power-law distributions.

We thank Einar Hinrichsen, Amnon Aharony, Paul Meakin, and Alexandar Birovljev for stimulating discussions and gratefully acknowledge support by VISTA, a research cooperation between the Norwegian Academy of Science and Letters and Den norske stats oljeselskap a.s. (STATOIL) and by NAVF, the Norwegian Research Council for Science and the Humanities.

[1] R. Lenormand, E. Touboul, and C. Zarcone, J. Fluid Mech. **189**, 165 (1988); R. Lenormand and C. Zarcone, Phys. Rev. Lett. **54**, 2226 (1985).
[2] J. Feder, *Fractals* (Plenum, New York, 1988).
[3] B. B. Mandelbrot, *The Fractal Geometry of Nature* (Freeman, San Francisco, 1982).
[4] K. J. Måløy, J. Feder, and T. Jøssang, Phys. Rev. Lett. **55**, 2688 (1985).
[5] K. J. Måløy, F. Boger, J. Feder, T. Jøssang, and P. Meakin, Phys. Rev. A **36**, 318 (1987).
[6] U. Oxaal, M. Murat, F. Boger, A. Aharony, J. Feder, and J. Jøssang, Nature (London) **329**, 32 (1987).
[7] L. Furuberg, J. Feder, A. Aharony, and T. Jøssang, Phys. Rev. Lett. **61**, 2117 (1988).
[8] S. Roux and E. Guyon, J. Phys. A **22**, 3693 (1989).
[9] D. Wilkinson and J. F. Willemsen, J. Phys. A **16**, 3365 (1983).
[10] W. B. Haines, J. Agr. Sci. **20**, 97 (1930).
[11] J. C. Melrose, Soc. Petr. Eng. J. **5**, 259 (1965).
[12] N. R. Morrow, Ind. Eng. Chem. **62**, 32 (1970).
[13] A. H. Thompson, A. J. Katz, and R. A. Raschke, Phys. Rev. Lett. **58**, 29 (1987).
[14] A. J. Katz, A. H. Thompson, and R. A. Raschke, Phys. Rev. A **38**, 4901 (1988).
[15] J. N. Roux and D. Wilkinson, Phys. Rev. A **37**, 3921 (1988).
[16] D. Stauffer, *Introduction to Percolation Theory* (Taylor & Francis, London, 1985).
[17] J. F. Gouyet, J. Phys. A **168**, 581 (1990).
[18] A. Birovljev, L. Furuberg, J. Feder, T. Jøssang, K. J. Måløy, and A. Aharony, Phys. Rev. Lett. **67**, 584 (1991).